Local measurement of vortex statistics in quantum turbulence

Eric Woillez, Philippe-E Roche

Local measurement of vortex statistics in quantum turbulence

Eric Woillez and Philippe-E. Roche

Univ. Grenoble Alpes, CNRS, Institut NEEL, F-38042 Grenoble, France

PACS 67.25.dk – Vortices and turbulence
PACS 47.37.+q – Hydrodynamic aspects of superfluidity: quantum fluids
PACS 67.25.dg – Transport, hydrodynamics, and superflow

Abstract – The density fluctuations of quantum vortex lines are measured in a turbulent flow of superfluid He, at temperatures corresponding to superfluid fraction of 16%, 47% and 81%. The probe is a micro-fabricated second sound resonator that allows for local and small-scale measurements in the core of the flow, at a 10-mesh-size behind a grid. Remarkably, all the vortex power spectra collapse on a single master curve, independently from the superfluid fraction and the mean velocity. By contrast with previous measurements, we report an absence of power law scaling of the power spectra. The vortex density probability distributions are found to be strongly skewed, similarly to the vorticity distributions observed in classical turbulence. Implications of those results are discussed.

Introduction. – At zero temperature, quantum fluids exhibit two fascinating superfluid properties [1] : the absence of viscous dissipation and the concentration of its vorticity along vortex lines, of atomic diameter in the case of ^{4}He vortices. Besides, the vortices are quantized in the sense that the circulation of velocity around one vortex has a fixed value ($\kappa \simeq 10^{-7}\mathrm{m}^2\mathrm{s}^{-1}$ in ^{4}He). At finite temperature, the superfluid behaves as if it experienced friction with a background viscous fluid, called the "normal fluid". The relative mass density of the superfluid ρ_s/ρ (where ρ is the total mass density) decreases from one at 0 K to zero at the superfluid transition temperature ($T_\lambda \simeq 2.18$ K in ^{4}He), suggesting a possible continuous cross-over between the properties of quantum and classical hydrodynamics.

These peculiar dissipation and vortical properties offer unique opportunities to revisit open questions in classical turbulence. Thus, the last two decades have seen the emergence a new research area applying the methodology and tools of classical turbulence to quantum flows [2], and in particular the statistical study of local fluctuations in highly turbulent canonical flows such as von Kármán, wakes and grid flows [3].

Local velocity statistics have been successfully probed with a variety of anemometers in highly turbulent flows, and similarities have been systematically found between quantum and classical turbulence (eg. [4–7]). This was attributed to a locking of the superfluid and normal fluid at large and intermediate flow scales, resulting in an apparent single-fluid viscous dynamics [3]. Still, the smallest scales of the flow -where quantum effects prevail- could not yet be resolved with existing anemometers [1]).

To circumvent this shortcoming of anemometers, two alternative types of probe have explored the statistics of small scale features of intense quantum turbulence.

First, using parietal pressure probes, the statistics of vorticity filaments in classical turbulence have been compared with their quantum counterparts: superfluid vortex bundles. Here again, a strong similarity between both types of turbulence was found [9].

Second, using "second sound tweezers", the spectrum of local density of superfluid vortex lines $\mathcal{L}$ has been measured [10] for $\rho_s/\rho \simeq 0.84$. Unexpectedly, the spectrum was consistent with a $\sim f^{-5/3}$ power law at intermediate scales, at odds with the spectrum of the absolute value of vorticity in classical turbulence. This spectral observation, studied numerically [11,12] and theoretically [13–15], has been up to now the only [2] existing experimental constrain for the small scale closure of the models of quantum hydrodynamics.

The present study reports the first statistical characterisation of local vortex line density (VLD) statistics in well-controlled highly turbulent flow, and over a wide range of

[1] for a recent attempt, see eg. [8]

[2] Literature also reports experimental [16] and numerical [17–21] spectra of the vortex line density spatially integrated across the whole flow. Still, spectra of such "integral" quantities differ in nature from the spectra of local quantities, due to strong filtering effects of spatial fluctuations.

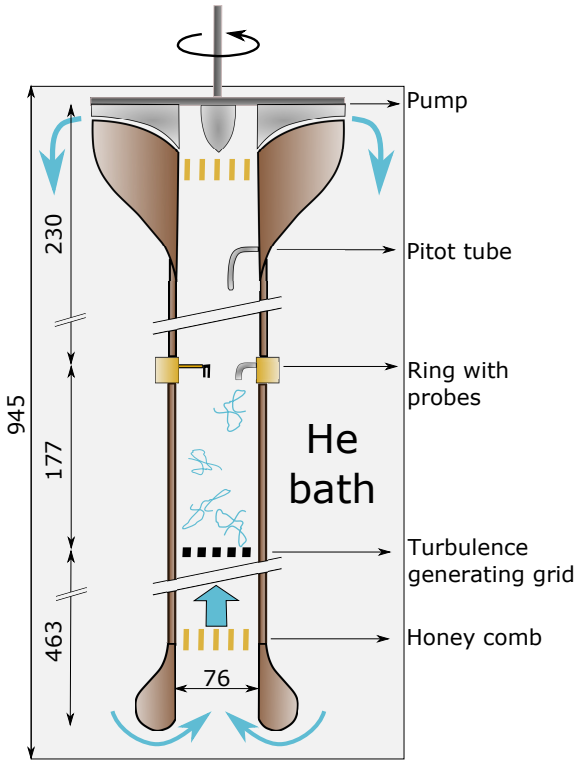

Fig. 1: Sketch of the flow and the experimental setup with probes.

ρ_s/ρ spanning from 0.16 to 0.81.

Experimental setup. – The experimental setup has been described in details in a previous publication [7], and we only review in this section the major modifications. The setup consists in a wind tunnel inside a cylindrical cryostat (see Fig. 1) filled with He-II. The flow is continuously powered by a centrifugal pump located at the top of the tunnel. At the bottom, an optimized 3D-printed conditioner ensures a smooth entry of the fluid, without boundary layer detachment, inside a pipe of $\Phi = 76$ mm inner diameter. Spin motion is broken by radial screens built in the conditioner. The fluid is then "cleaned" again by a 5-cm-long and 3-mm-cell honeycomb. The mean flow velocity U is measured with a Pitot tube located 130 mm upstream the pipe outlet. We allow a maximal mean velocity $U = 1.3$ m/s inside the pipe to avoid any cavitation effect with the pump.

The main new element compared to the previous design is a mono-planar grid located 177 mm upstream the probes to generate turbulence. The grid has a $M = 17$ mm mesh with square bars of thickness $b = 4$ mm, which gives a porosity of $\beta = (1 - b/M)^2 \approx 0.58$.

The choice to position the probes at a distance $\sim 10M$ downstream the grid is the result of a compromise between the desire to have a "large" turbulence intensity, and the necessity to leave enough space for turbulence to develop between the grid and the probes. In-situ measurements of the mean vortex line density can be used to indirectly (via Eq. 6) give an estimation of the the turbulence intensity $\tau = u^{\rm rms}/U \simeq 12 - 13\%$ (where $u^{\rm rms}$ is the standard deviation of longitudinal velocity component). We present the results later in Fig. 5). For comparison, Vita and co. [22] report a turbulence intensity around $\tau = 9\%$ percents at $10M$ in a classical grid flow of similar porosity. The difference between both values of τ could originate from a prefactor uncertainty in Eq. (6) or from differences in flow design (e.g. the absence of a contraction behind the honeycomb). This difference has no important consequences for the present study devoted to the measure of quantum vortex statistics, and was not further examined.

The longitudinal integral length scale of the flow $H \simeq 5.0$ mm is assessed by fitting velocity spectra (see bottom panel of Fig.6) with the von Kármán formula (eg. see [22]). For comparison, the integral scale reported for the similar grid in [22], once rescaled by the grid size, gives a nearby estimate of 7.4 mm.

The Reynolds number Re defined with $u^{\rm rms}H$ and the kinematic viscosity 1.8×10^{-8} m^{2}s^{-1} of liquid He just above T_λ, is $Re = 2.5 \times 10^4$ for $U = 1$ m/s. Using standard homogeneous isotropic turbulence formula [23], this Re corresponds to a Taylor scale Reynolds number $R_\lambda = 690$ (for $\tau = 9\%$ and $H = 5$ mm). This gives an indication of turbulence intensity of the flow below T_λ.

Temperature of the helium bath is set via pressure regulation gates. The exceptional thermal conductivity of He-II ensures an homogeneous temperature inside the bath for $T < T_\lambda$. Two Cernox thermometers, one located just above the pump, the other one on the side of the pipe close to the probes, allow for direct monitoring of T.

Probes. – We have four probes to measure quantum turbulence characteristics. The first one is a miniature Pitot tube that allows for *in situ* measurements of velocity fluctuations for monitoring purposes. It is composed of a capillary tube of 0.8 mm diameter and a micro-machined differential piezo-resistive pressure transducer at its close end (see Fig. 2).

The three other probes are micro-fabricated second sound tweezers of the millimeter size according to the same principle as in [10]. As displayed in the inset of Fig. 2, the tweezers are composed of one heating plate and one thermometer plate facing each other and thus creating a resonant cavity for thermal waves. The heating plate generates a stationary thermal wave of the order of 0.1 mK between the plates, the amplitude of which can be recorded by the thermometer plate. Two major improvements have been done compared to the tweezers in [10] : first, the lengths of the arm supporting the plates has been increased to 12.5 mm to avoid blockage effects. Second, two notches are done in the arms to avoid interference due to additional reflections of the thermal wave on the arms. Further details will be given in a future publication.

In the presence of He flow, a variation of the amplitude and phase of the thermal wave can be observed. This variation is due to two main physical effects. The presence of

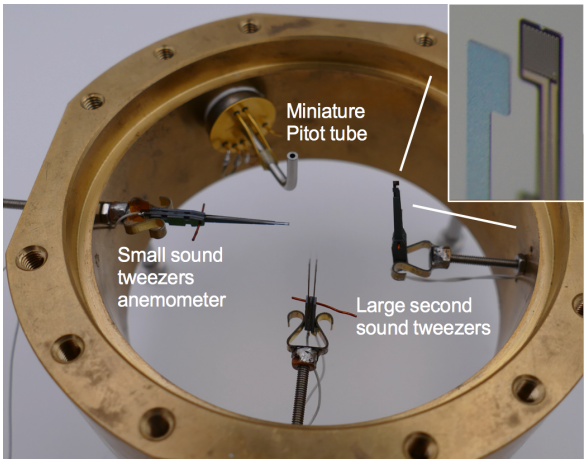

Fig. 2: Ring with probes. The inset is a zoom on the heating and the thermometer plates of a second sound tweezers.

quantum vortex lines inside the cavity causes an attenuation of the wave [24, 25] with a very minor phase shift [26]. This attenuation can be very accurately modelized by a bulk dissipation coefficient inside the cavity denoted ξ_L. The second effect is a ballistic advection of the wave out of the cavity. It is related to both an attenuation of the temperature oscillation and an important phase shift. Depending on the flow mean velocity U, the size of the tweezers, and the frequency of the wave, one of these two effects can overwhelm the other. We have thus designed two models of tweezers: one model to take advantage of the first effect to measure the vortex lines density (VLD), and the other one to take advantage of the second effect to measure the velocity.

The two largest tweezers displayed in Fig. 2 are designed to measure the quantum vortex lines density. The plates size is $l = 1$ mm and the gaps between the plates are $D = 1.32$ mm and $D = 0.83$ mm respectively. The plates face each other with positioning accuracy of a few micrometers. The tweezers are oriented parallel to the flow (see Fig. 2) to minimize the effect of ballistic advection of the wave.

The smallest tweezers displayed in Fig. 2 are designed to measure the velocity fluctuations parallel to the mean flow. The two plates have a size $l = 250$ μm, and are separated by a gap of $D = 0.431$ mm. The tweezers are oriented perpendicular to the mean flow (see Fig. 2) with an intentional lateral shift of the heater and the thermometer of about $l/2$. This configuration is expected to maximize the sensitivity to ballistic advection, and thus to velocity fluctuations. However, due to excessive heating of this probe, we were not able to calibrate it reliably. Consequently we do not use it to estimate the turbulence intensity. The velocity spectrum (in arbitrary units) of this probe is displayed in the bottom panel of Fig 6. This anemometer is mostly used in the present study to assess the integral scale and qualitatively check the stability of the flow.

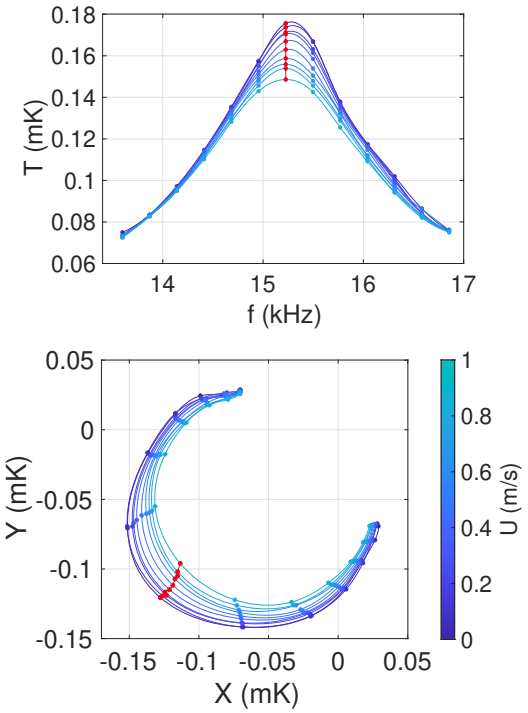

Fig. 3: **Top:** second sound resonance of the tweezers around 7.6 kHz. The value of U increases from top curve to bottom curve. The vertical axis gives the amplitude of the thermal wave in K. **Bottom:** representation of the same resonance in phase and quadrature.

Method. – Figure 3 displays a resonance of a large tweezers at frequency $f_0 = 15.2$ kHz, for increasing values of the mean velocity. The temperature oscillation T measured by the thermometer is demodulated by a Lock-in amplifier NF LI5640. T can be accurately fitted by a classical Fabry-Perot formula

$$T = \frac{A}{\sinh\left(i\frac{2\pi(f-f_0)D}{c_2} + \xi D\right)} \tag{1}$$

where f_0 is the resonant frequency for which the wave locally reaches its maximal amplitude, c_2 is the second sound velocity, A is a parameter to be fitted, and ξ is related to the energy loss of the wave in the cavity. The top panel of Fig. 3 displays the amplitude of the thermal wave (in mK) as a function of the frequency, and the bottom panel shows the same signal in phase and quadrature. When the frequency is swept, the signal follows a curve close to a circle crossing the point of coordinates $(0, 0)$. Fig. 3 clearly shows that the resonant peak shrinks more and more when U increases, which is interpreted as attenuation of the wave inside the cavity. The red points display the attenuation of the signal at constant value of f. It can be seen on the bottom panel that the variation of the signal is close to a pure attenuation, that is, without phase shift. ξ can be decomposed as

$$\xi = \xi_0 + \xi_L \tag{2}$$

where ξ_0 is the attenuation factor when $U = 0$ m/s and ξ_L is the additional attenuation created by the presence of quantum vortex lines inside the cavity. ξ_L is the signal of interest as it can be directly related to the vortex lines density (VLD) using the relation

$$\xi_L = \frac{B\kappa L_\perp}{4c_2}, \quad (3)$$

$$L_\perp = \frac{1}{\mathcal{V}}\int \sin^2\theta(l)\mathrm{d}l \quad (4)$$

where B is the first Vinen coefficient, $\kappa \approx 9.98 \times 10^{-8}$ m^2/s is the quantum of circulation, $\mathcal{V}$ is the cavity volume, l is the curvilinear abscissa along the vortex line, $\theta(l)$ is the angle between the vector tangent to the line and the direction perpendicular to the plates. We note that the summation is weighted by the distribution of the second sound nodes and antinodes inside the cavity and does not exactly corresponds to a uniform average but we neglect this effect in the following. Our aim is to measure both the average value and the fluctuations of $L_\perp$, as a function of U and the superfluid fraction.

The method goes as follows: first, we choose a resonant frequency f_0 where the amplitude of the signal has a local maximum and we fix the frequency of the heating to this value f_0. Then we vary the mean velocity U and we record the response of the thermometer plate in phase and quadrature. The measurements show that the velocity-induced displacement in the complex plane follows a straight line in a direction $\overrightarrow{e}$ approximately orthogonal to the resonant curve. Expressions (1-2) give ξ_L from the measured amplitude T by [10]

$$\xi_L = \frac{1}{D}\mathrm{asinh}\left(\frac{\mathrm{A}}{\mathrm{T}}\right) - \xi_0. \quad (5)$$

The colored dots of Fig. 4 illustrate the fluctuations of the signal in phase and quadrature, for different values of U. The average signal moves in the direction of the attenuation axis. The figure also shows a part of the resonant curve for $U = 0$. The fluctuations have two components in the plane, both associated with different physical phenomena. Fluctuations in the direction tangent to the resonant curve can be interpreted as a variation of the acoustic path $\frac{2\pi(f-f_0)D}{c_2}$ without attenuation of the wave. Those fluctuations can occur for example because the two arms of the tweezers vibrate with submicron amplitude, or because the temperature variations modify the second sound velocity c_2. To isolate only the fluctuations associated to attenuation by the quantum vortices, we split the signal into a component along the attenuation axis, and another one along the acoustic path axis. We then convert the displacement along the attenuation axis into vortex line density (VLD) using expressions (3-5).

Results. – As a check of the validity of our approach, we measured the average response of the second sound tweezers as a function of the mean velocity U. According to literature [27], we were expecting the scaling

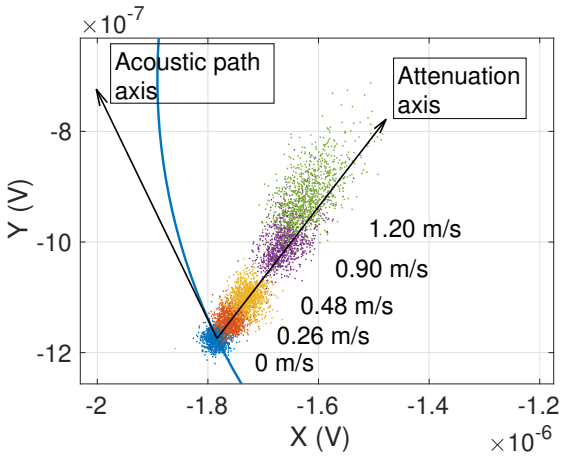

Fig. 4: Fluctuations of the thermal wave in phase and quadrature. The colored clouds show the fluctuations of the signal, for different values of U. The blue curve shows the resonance for $U = 0$ m/s. The fluctuations tangent to the resonant curve are created by a variation of the acoustic path. The quantum vortices are associated to attenuation of the wave and create a displacement along the attenuation axis.

$\langle L_\perp\rangle^2 \propto U^3$, with a prefactor related to the flow main characteristics. The function $\langle L_\perp\rangle$ was thus measured for a range $0.4 < U < 1.25$ m/s with a time averaging over 300 ms, at the three different temperatures 1.65 K, 1.99 K and 2.14 K.

An effective superfluid viscosity ν_{eff} is customarily defined in quantum turbulence by $\epsilon = \nu_{\mathrm{eff}}(\kappa\mathcal{L})^2$ where ϵ is the dissipation and $\mathcal{L} = 3\langle L_\perp\rangle/2$ is the averaged VLD (we assume isotropy of the tangle) [28]. For large R_λ homogeneous isotropic flows, we also have $\epsilon \simeq 0.79\,U^3\tau^3/H$ (eg see [23] p.245), which entails

$$\tau^3 \simeq 2.85\frac{\nu_{\mathrm{eff}}H\kappa^2\langle L_\perp\rangle^2}{U^3} \quad (6)$$

Using Eq. (6), we compute the turbulence intensity as a function of U, for the three considered temperatures. The result is displayed in Fig. 5. The figure shows that the turbulence intensity reaches a plateau of about 12% above 0.8 m/s, a value in accordance with the turbulence intensity of 9% reported in [22] for a grid turbulence with similar characteristics. The figure also confirms that the expected scaling $\langle L_\perp\rangle^2 \propto U^3$ is reached in our experiment for the range of velocities $U > 0.8$ m/s.

The temperature-dependent viscosity ν_{eff} in Eq. (6) has been measured in a number of experiments (eg see compilations in [15, 27, 29]). Still, the uncertainty on its value exceeds a factor 2. For the temperatures 1.65 K and 1.99 K, we used the average values 0.2κ and 0.25κ. By lack of reference experimental value of ν_{eff} above 2.1 K, we determined it by collapsing the $\tau(U)$ datasets obtained at 2.14 K with the two others. We found the value $\nu_{\mathrm{eff}} \approx 0.5\kappa$

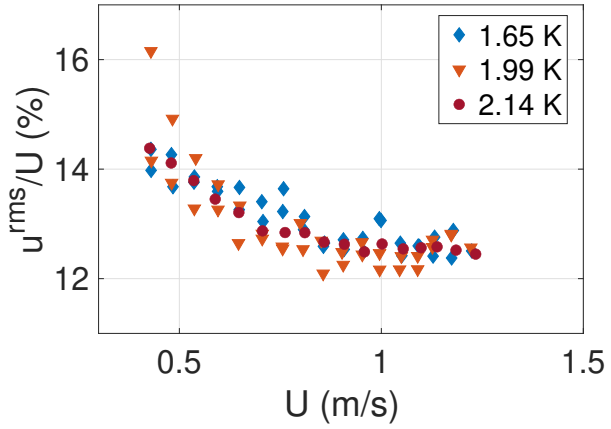

Fig. 5: Indirect measurement of the turbulence intensity $\tau = u^{\rm rms}/U$ as a function of U using Eq. (6). The three different symbols correspond to three values of the mean temperature.

at 2.14 K.

Assuming isotropy of the vortex tangle, the value of $\mathcal{L}$ gives a direct order of magnitude of the inter-vortex spacing $\delta = 1/\sqrt{\mathcal{L}}$. We find $\delta \approx 5$ μm at 1.65 K and a mean velocity of 1 m/s. This shows the large scale separation between the inter-vortex spacing and the flow integral scale H, a confirmation of an intense turbulent regime.

Fig. 6 presents the main result of this letter. We display on the top panel the VLD power spectral density $P_L(f)$ of $L_\perp/\langle L_\perp\rangle$. With this definition, the VLD turbulence intensity $L_\perp^{\rm rms}/\langle L_\perp\rangle$ is directly given by the integral of $P_L(f)$. We have measured the VLD fluctuations at the temperatures $T = 1.65$ K and superfluid fraction $\rho_S/\rho = 81\%$, $T = 1.99$ K and $\rho_S/\rho = 47\%$, $T = 2.14$ K and $\rho_S/\rho = 16\%$. At each temperature, the measurement was done for at least two different mean velocities.

The first striking result is the collapse of all the spectra independently of the temperature, when properly rescaled using f/U as coordinate (and $P_L(f)\times U$ as power spectral density to keep the integral constant). The VLD spectrum does not depend on the superfluid fraction even for vanishing superfluid fractions, when T comes very close to T_λ. Only one measurement with one of the large tweezers at $T = 1.650$ K has given a slight deviation from the master curve of the VLD spectra: it is displayed as the thin grey curve in Fig. 6. We have no explanation for this deviation but did not observe this particular spectrum with the second tweezers, and neither at any other temperature.

Second, the VLD spectrum has no characteristic power-law decay. We only observe that the spectrum follows an exponential decay approximately above $f/U > 100$ m^{-1}. This strongly contrasts with the velocity spectrum obtained with the small second sound tweezers anemometer (see bottom panel), which displays all the major features expected for a velocity spectrum in classical turbulence: it has a sharp transition from a plateau at large scale to a power law scaling close to $-5/3$ in the inertial scales of the turbulent cascade. A fit of the transition using the von Kármán expression (see [22]) gives the value $H = 5$ mm for the longitudinal integral scale. As a side remark, the apparent cut-off above 10^3 m^{-1} is an instrumental frequency cut-off of the tweezers.

We find a value of the VLD turbulent intensity close to 20%, which is significantly higher than the velocity turbulence intensity. We also checked that we obtain the same VLD spectrum using different resonant frequencies f_0.

Our measurements are limited by two characteristic frequencies. First, the tweezers average the VLD over a cube of side l, which means that our resolution cannot exceed $f/U > 1/l$. For the large tweezers, this sets a cut-off scale of 10^3 m^{-1}, much larger than the range of inertial scales presented in top panel of Fig. 6. Second, the frequency bandwidth of the resonator decreases when the quality factor of the second sound resonance increases. This again sets a cut-off scale given by $f/U = \xi_0 c_2/(2U)$. The worst configuration corresponds to the data obtained at 2.14 K and $U = 1.2$ m/s where the cut-off scale is about 600 m^{-1}. For this reason, the VLD spectra of Fig. 6 are conservatively restricted to $f/U < 300$ m^{-1} which allows to resolve about one and a half decade of inertial scales.

Figure 7 displays some typical PDF of the rescaled VLD fluctuations $L_\perp/\langle L_\perp\rangle$ in semilogarithmic scale, for the three considered temperatures. The PDF have been vertically shifted by one decade from each other for readability. The figure shows a strong asymmetry at all temperatures, with a nearly Gaussian left wing, and an exponential right wing. Contrarily to the VLD spectra, the PDF do not accurately collapse at different velocities and temperatures: only the global asymmetric shape seems to be a robust feature. We do not see a clear trend when increasing the temperature and/or the mean velocity. By contrast, the dotted curve in Fig. 7 displays one PDF of the small tweezers anemometer at 1.65 K, for which the mean has been shifted and the variance rescaled. It can be seen that the general shape of this latter PDF is much more symmetric and closer to a Gaussian as expected for a PDF of velocity fluctuations.

Discussion and conclusion. – In the present paper, we have investigated the temperature dependence of the statistics of the local density of vortex lines (VLD) in quantum turbulence. About one and a half decade of inertial scales of the turbulent cascade was resolved. We measure the VLD mean value and deduce from Eq. (6) the turbulence intensity (Fig. 5), we report the VLD power spectrum (Fig. 6), and the VLD probability distribution (Fig. 7). Whereas the VLD mean value at different temperatures confirms previous numerical [11,27] and experimental studies [27], the spectral and PDF studies are completely new. Only one measurement of the VLD fluctuations had been done previously [10] but in an ill-defined flow around 1.6K.In the present work, we have used a grid turbulence, which is recognized as a reference flow for isotropic turbulence.

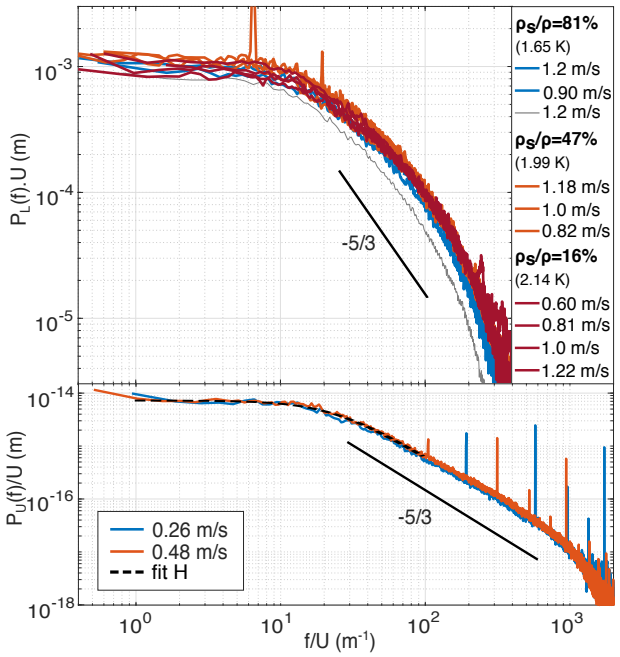

Fig. 6: **Top:** Power spectral density of the projected vortex line density (VLD) $L_\perp$, obtained with the large second sound tweezers, for different values of U and temperatures. All measured spectra collapse using the scaling f/U and $P_L(f) \times U$. The fluctuations have been rescaled by the mean value of the VLD such that the integral of the above curves directly give the VLD turbulence intensity. **Bottom:** Power spectral density of the uncalibrated velocity signal obtained from the second sound tweezers anemometer, for two values of U at 1.65 K. The spectra collapse using the scaling f/U for the frequency and $P_U(f)/U$ for the spectral density. The straight line displays the $-5/3$ slope which is expected for a classical velocity spectrum in the inertial range of the turbulent cascade. The dotted line is a fit using the von Kármán expression (see [22]) to find the integral scale H.

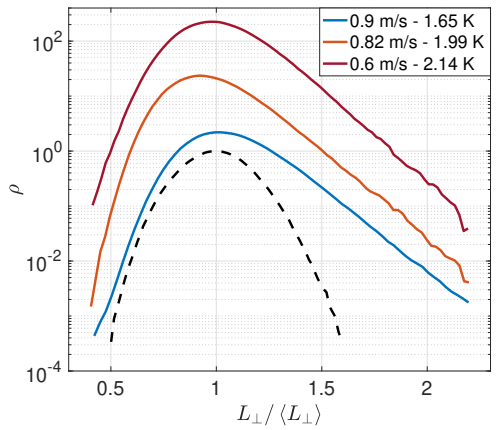

Fig. 7: Normalized probability distributions of the VLD fluctuations obtained at three temperatures. The PDF have been shifted by one decade from each other for readability. By comparison, the dotted black curve displays a rescaled PDF obtained with the small tweezers measuring velocity.

To conclude, we discuss below three main findings:

1. A master curve of the VLD spectra, independent of temperature and mean velocity.
2. An absence of power law scaling of the VLD spectra.
3. A global invariant shape of the strongly skewed PDF.

The mean VLD gives the inter-vortex spacing, and thus tells how much quantum vortices are created in the flow, whereas the PDF and spectra tell how those vortices are organized in the flow. From 2.14K to 1.65K, our results confirm that the inter-vortex spacing only weakly decreases, by less than 23% for a 5-times increase of the superfluid fraction. In other words, the superfluid fraction has a limited effect on the creation of quantum vortices. The current understanding of the homogeneous isotropic turbulence in He-II is that the superfluid and normal fluid are locked together at large and intermediate scales where they undergo a classical Kolmogorov cascade [3]. The experimental evidences are based on the observation of classical velocity statistics using anemometers measuring the barycentric velocity of the normal and superfluid components. Here, the temperature-independence of (normalized) VLD spectra supports this general picture, by reminiscence of a similar property of He-II velocity spectra.

However, in contrast with velocity, this also reveals some temperature-independence of scales *smaller* than the probe spatial resolution. For instance, positive and negative velocity fluctuations (e.g like those around a vortex core) smaller than the probe resolution are strongly damped by averaging , while our VLD probe returns the sum of a positive quantity and keeps track of the small scales fluctuations. Besides, the intermediate scales of 1D vorticity spectra in classical turbulence are related to the velocity spectrum at small scales (eg. see [30]) and the same property is expected to hold in quantum turbulence, in a form yet to be detailed.

The observed temperature-independence of spectra is thus constraining for the delicate modeling of the small scales of quantum turbulence, in particular to develop mathematical closures for the continuous description of He-II (eg. see [31]).

Second, the absence of power law scaling apparently contrasts with the spectra reported as "compatible with" a $f^{-5/3}$ scaling in [10]. We have no definite explanation for this difference. Still, we note that the averaged spectral decrease reported in the present study over one and a half decade of inertial scales is close to the decrease reported in [10] over a similar range. Speculatively, the absence of complete development of turbulence at $10M$ from the grid could result in residual imbalance between flow scales, or from some memory effect associated with flow forcing at the grid.

As a discussion of the third statement, we compare our results with those of numerical simulations done in classical turbulence. The absolute value of vorticity can be seen

as a classical counterpart to the VLD. The work of Iyer and co. [32] for example, displays some enstrophy PDF from high resolution DNS, that can be compared to the PDF of Fig. 7. It can be seen in [32] that such PDF are not universal and depend on the Re number and the averaging scale: this probably justifies why the distributions of Fig. 7 do not collapse. At small scale, the enstrophy PDF are strongly asymmetric and will ultimately converge to a Gaussian distribution when averaged over larger and larger scales. Although our tweezers average the VLD over a size much larger than the inter-vortex spacing, they are small enough to sense short-life intense vortical events, typical of small scale phenomenology in classical turbulence. Thus, the strong asymmetry of the PDF supports the analogy between VLD and enstrophy (or its square root) and shows the relevance of VLD statistics to explore the small scales of quantum turbulence.

A side result of the present work is to obtain the relative values of the empirical coefficient $\nu_{\text{eff}} = \epsilon(\kappa\mathcal{L})^{-2}$ at the three considered temperatures. Models and simulations predict that ν_{eff} should steeply increase close to T_λ (see [15,27,29] and ref. within), in apparent contradiction with the only systematic experimental exploration [33]. We found in Fig. 5 that the effective viscosity ν_{eff} is twice larger at 2.14K than at 1.99K. To the best of our knowledge, our estimate $\nu_{\text{eff}}(2.14K) \simeq 2\,(\pm 0.25) \times \nu_{\text{eff}}(1.99K)$ is the first experimental hint of such an effective viscosity increase.

* * *

We warmly thank Jérôme Valentin for the process development and micro-fabrication of the components of the sensors, B. Chabaud for support in upgrading the wind-tunnel and P. Diribarne, E. Lévêque and B. Hébral for their comments. We thank K. Iyer with his co-authors for sharing data on the statistics of spatially averaged enstrophy analyzed in [34]. Financial support from grants ANR-16-CE30-0016 (Ecouturb) and ANR-18-CE46-0013 (QUTE-HPC).

REFERENCES

[1] Donnelly R. J., *Quantized Vortices in Helium-II* Cambridge Studies in Low Temperature Physics (Cambridge University Press, Cambridge) 1991.
[2] *Quantum turbulence special feature* (2014).
[3] Barenghi C. F., L'vov V. S. and Roche P.-E., *PNAS*, **111** (2014) 4683.
[4] Maurer J. and Tabeling P., *Europhys. Lett.*, **43** (1998) 29.
[5] Salort J. *et al.*, *Phys. Fluids*, **22** (2010) 125102.
[6] Salort J., Chabaud B., Lévêque E. and Roche P.-E., *EPL*, **97** (2012) 34006.
[7] Rusaouen E., Chabaud B., Salort J. and Roche P.-E., *Phys. Fluids*, **29** (2017) 105108.
[8] Salort J. *et al.*, *Search for an Experimental Signature of Quantum Turbulence in Velocity Spectra* working paper or preprint (Feb. 2021).
[9] Rusaouen E., Rousset B. and Roche P.-E., *EPL*, **118** (2017) 14005.
[10] Roche P.-E., Diribarne P., Didelot T., Français O., Rousseau L. and Willaime H., *EPL (Europhysics Letters)*, **77** (2007) 66002.
[11] Salort J., Roche P.-E. and Lévêque E., *EPL (Europhysics Letters)*, **94** (2011) 24001.
[12] Baggaley A. W., Barenghi C. F., Shukurov A. and Sergeev Y. A., *EPL*, **98** (2012) 26002.
[13] Roche P.-E. and Barenghi C. F., *EPL*, **81** (2008) 36002.
[14] Nemirovskii S. K., *Phys. Rev. B*, **86** (2012) 224505.
[15] Boué L., L'vov V. S., Nagar Y., Nazarenko S. V., Pomyalov A. and Procaccia I., *Phys. Rev. B*, **91** (2015) 144501.
[16] Bradley D. I., Fisher S. N., Guénault A. M., Haley R. P., O'Sullivan S., Pickett G. R. and Tsepelin V., *Phys. Rev. Lett.*, **101** (2008) 065302.
[17] Fujiyama S. and Tsubota M., *J. Low Temp. Phys.*, **158** (2010) 428.
[18] Baggaley A. W. and Barenghi C. F., *Physical Review B*, **84** (2011) 020504.
[19] Baggaley A. W., Laurie J. and Barenghi C. F., *Phys. Rev. Lett.*, **109** (2012) 205304.
[20] Baggaley A. W., Tsepelin V., Barenghi C. F., Fisher S. N., Pickett G. R., Sergeev Y. A. and Suramlishvili N., *Phys. Rev. Lett.*, **115** (2015) 015302.
[21] Tsepelin V., Baggaley A. W., Sergeev Y. A., Barenghi C. F., Fisher S. N., Pickett G. R., Jackson M. J. and Suramlishvili N., *Phys. Rev. B*, **96** (2017) 054510.
[22] Vita G., Hemida H., Andrianne T. and Baniotopoulos C. C., *Journal of Wind Engineering and Industrial Aerodynamics*, **178** (2018) 91.
[23] Pope S., *Turbulent Flows* (Cambridge University Press) 2000.
[24] Donnelly R. J., *Physics Today*, **37** (1984) S34.
[25] Varga E., Jackson M., Schmoranzer D. and Skrbek L., *J. Low Temp. Phys.*, **197** (2019) 130.
[26] Miller R., Lynall I. and Mehl J., *Physical Review B*, **17** (1978) 1035.
[27] Babuin S., Varga E., Skrbek L., Lévêque E. and Roche P.-E., *EPL*, **106** (2014) 24006.
[28] Vinen W. F. and Niemela J. J., *J. Low Temp. Phys.*, **128** (2002) 167.
[29] Gao J., Guo W., Yui S., Tsubota M. and Vinen W., *Phys. Rev. B*, **97** (2018) 184518.
[30] Antonia R., Shafi H. and Zhu Y., *Phys. Fluids*, **8** (1996) 2196.
[31] Nemirovskii S. K., *J. Low Temp. Phys.*, **201** (2020) 254.
[32] Yeung P., Zhai X. and Sreenivasan K. R., *Proc. Natl. Acad. Sci.*, **112** (2015) 12633.
[33] Stalp S., Niemela J. J., Vinen W. J. and Donnelly R. J., *Phys. Fluids*, **14** (2002) 1377.
[34] Iyer K. P., Schumacher J., Sreenivasan K. R. R. and Yeung P. K., *New J. Phys.*, **21** (2019) 033016.